Receptor for Specific Detection of TKX 50 and Integration of the Switch On Fluorescence Responses into an IoT-Based Smart Device

Somnath Bej,*[a] Sourav Dutta,[a] Sheik Salim Pasha,[b] Anik K. De,[bc] Debmalya Roy,[d] Lopamudra Roy,[e] Ria Ghosh,[e] Amrita Banerjee,[e] Nivedita Pan,[e] Samir Kumar Pal,*[e] Sumit K. Pramanik,*[bc] and Amitava Das*[a]

[a]Department of Chemical Sciences, Indian Institute of Science Education and Research Kolkata, Mohanpur, West Bengal-741246, E-mail: amitava@iiserkol.ac.in

[b]CSIR-Central Salt & Marine Chemicals Research Institute, Bhavnagar 364002, Gujarat, India.

[c]Academy of Scientific and Innovative Research (AcSIR), Ghaziabad – 201002, India, Email: sumitpramanik@csmcri.res.in

[d]Defence Material and Stores Research and Development Establishment, Kanpur, UP, India, E-Mail: droy.dmsrde@gov.in

[e]Department of Chemical, Biological & Macromolecular Sciences, S N Bose National Centre for Basic Sciences, JD Block, Sector III, Salt Lake City, Kolkata- 700106, E-mail: skpal@bose.res.in

Abstract: TKX-50 is one of the new generation secondary explosives that have been introduced recently in the modern weapon system due to its low impact/friction sensitivity, and high thermal stability, density, and detonation velocity. In response to the growing concerns about the illegitimate use of certain explosives by various organized agencies, there is an urgent need for effective recognition and quantification of such explosives for efficient security screening, homeland security, and human safety. However, such a detection process must be free from the scope of any false positive or false negative response. Herein, we report a new polymeric receptor derived from hydroxyl-functionalized tetra phenyl ethylene (TPE-OH) for specific detection of TKX 50 by monitoring its fluorescence-ON responses on binding to TKX 50. A details spectroscopic (steady-state and time-resolved fluorescence) studies confirm that the fluorescence 'ON' response is attributed to an interrupted non-radiative deactivation process for TKX-50 bound receptor **IV** (K_a = 2.4 x 10^3 M^{-1}), which otherwise is operation in receptor **IV**. A control monomeric derivative of TPE-OH is also synthesized and is used for our studies to further corroborate our proposition. Furthermore, a smart and user-friendly IoT-based device has been developed, allowing the integration of optical responses into a digital output. This lightweight portable device enables IoT-based remote detection and is appropriate for surveillance applications. To the best of our knowledge, examples of such smart integration of the optical responses to a user datagram protocol (UDP)-based Wi-Fi communication and data processing for remote monitoring of TKX 50 are scarce and in the contemporary literature.

Introduction: Terrorism is the threat to intimidate in the pursuit of political or ideological goals and is usually done by non-state actors who are not part of the government. This is the most direct asymmetric threat to humanity, the security of the global population, and international/ regional stability. Recent international events and regional political instabilities have contributed to the recent rise in various terror activities and fighting terrorism is a top priority for every single government agency. To maintain the in-land security, territorial integrity, and sovereignty of any country all countries need to look for higher explosives (HEs). The choice of such HEs is strictly driven by the recent emphasis on new types of detonators is driven by enhanced safety requirements, protection against unauthorized use, and environmental concerns, apart from the specific requirements set by users. Sensitivity and thermal stability are typically the crucial parameters for HEs for their safety in transport and storage.[1] Dihydroxylammonium 5,5′-bistetrazole-1,1′-diolate (TKX-50), contemporary state-of-the-art thermobaric explosives (TBXs) first reported in 2012, is an energetic ionic salt with low toxicity, high energy density, and low mechanical sensitivity, apart from the ease of synthesis using inexpensive organic compounds.[2] TKX-50 is a secondary explosive in modern weapon systems with low sensitivities (IS=20 J, FS=120 N) and good performance parameters at its theoretical maximum density (1.877 g cm−3 at 298 K).[3] The reported detonation velocity of TKX-50 is 9698 m/s, which is higher than RDX (250 m/s) and other HEs like ε-hexanitrohexaazaisowurtzitane (ε-CL-20, ~ 9455 m/s) or 1,1-diamino-2,2-dinitroethylene (FOX 7 ~ 8050 m/s). In addition, the impact sensitivity of TKX-50 (20 J) is lower than 2,4,6-trinitrotoluene (TNT, 15 J), and its friction sensitivity (120 N) is comparable to hexahydro-1,3,5-trinitro-1,3,5-triazine (RDX).[4] Considering the significance of its application potential in modern weapon systems, as well as its easy scalable synthesis, TKX 50 is one of the popular choices to induce fatal consequences at the target population or an establishment. Thus, a quick responsive, but authentic recognition and detection of TKX 50 has significance for homeland safety/security. This also enhances the possibility of soil or water body contamination in the vicinity of manufacturing plants, as well as in the areas associated with landmine detonations and leaching of abandoned weapon systems. All these add to adverse environmental effects and have triggered a large body of research for remediation and detection of explosives residues in soil and water bodies.[5] Detection of such explosives primarily depends on the use of FTIR/Resonance Raman spectrometer, Gas chromatogram, mass spectrometry, X-ray imaging, thermal neutron analysis, etc..[6] Deployment of such facilities along with skilled manpower is typically not conducive for in-filed monitoring and also raises the possibility for loss of human life, apart from the false negative or false positive responses as an instrumental-detection process artifact. As such detection techniques solely exploit respective spectral databases for all such registered suspected chemicals. We propose to exploit a fluorescence-based recognition strategy for specific sensing of TKX 50 in the presence of other explosives utilizing a 'fluorescence ON' based response of a molecular receptor.

Internet of Things (IoT) based frameworks have triggered a paradigm shift in monitoring changes in critical environmental parameters using appropriate sensors, microcontrollers, and IoT-based technology. We also propose to integrate the 'fluorescence ON' response in developing an IoT-based device that allows remote screening/monitoring of the explosive samples with no or minimal physical interference with the improvised explosive devices (IED) and explosive compounds.

A variety of materials, including luminescent compounds, metal–organic frameworks (MOFs), porous organic frameworks (POFs), covalent organic frameworks (COFs), and inorganic nanomaterials have been utilized for the detection of explosives, primarily nitro explosives (e.g. RDX, PA, TNT, PETN, etc.) only.[7] Even Two-dimensional lanthanide coordination polymer nanosheets have been used for the detection of FOX-7.[8] However, such examples of the detection of secondary explosives are rather scarce in the contemporary literature. Herein, we demonstrate a new polymeric backbone consisting of tetra phenyl ethylene (TPE) moieties (Scheme 1) for efficient and selective detection of TKX 50 based on the 'fluorescence ON' responses via non-radiative charge transfer processes. Furthermore, we have also developed a unique IoT-enabled smart electronic device that allows us to integrate the optical responses to a digital output for the detection of TKX 50. To the best of our knowledge, this is a unique example of an IoT-based device for the detection of TKX 50.

Results and discussion

In particular, our group is focusing on demonstrating a polymeric compound containing appropriate functionality that might be able to show selective detection of TKX 50 via changing its luminescent behavior with very fast sensitivity presenting through smart electronic devices. In this direction, a control compound **III** and a polymeric molecular receptor **IV** are prepared following scheme 1. Initially, compound **I** was synthesized from 4-hydroxybenzophenone as the starting material by utilizing McMurry coupling as per the literature report.[9] Formylation of compound **I** has been carried out by using hexamethyltetraamine and TFA to get compound **II** (Fig. S1- S4, ESI†). Furthermore, the monomeric compound **III** and polymeric compound **IV** were achieved by the reaction with compound **II** and corresponding amine-containing compounds respectively (Fig. S5- S14, ESI†). Detailed synthetic procedures have been described in the experimental section. All the synthesized compounds are characterized by usual spectroscopic, analytical, and microscopic techniques such as NMR, Mass (ESI-MS), Fourier transform infrared (FTIR), UV-Vis absorption, Photoluminescence (PL), X-ray photoelectron spectroscopy (XPS) analysis, Field emission scanning electron microscopy (FE-SEM), Transmission electron microscopy (TEM) etc. where ever applicable.

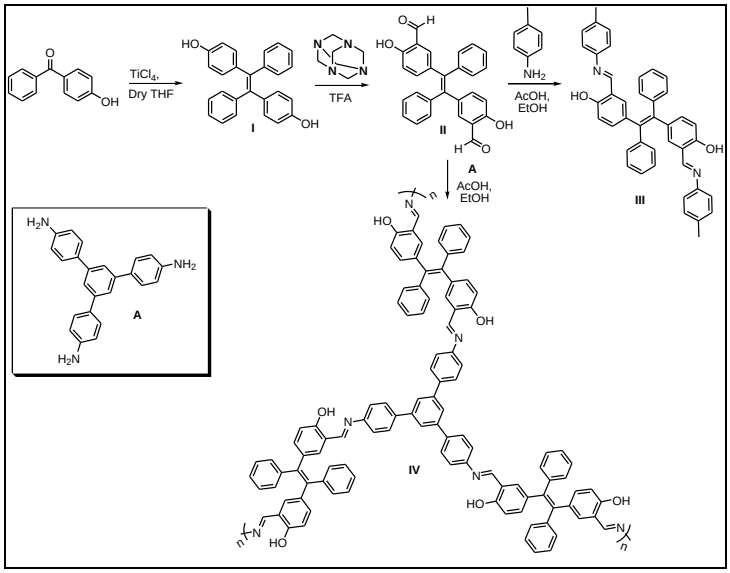

Scheme 1. Synthetic pathway of monomeric compound **III** and polymeric compound **IV**.

Photophysical study:

Primarily, the formation of imine functionalities in the monomeric (**III**) and polymeric (**IV**) compounds was established by FTIR studies (Fig. S7, ESI†, and Fig. 1A). Comparative FTIR spectra for **II** and **IV** are shown in ESI† (Fig. S12). The appearance of a new peak at ~1617 cm^{-1} due to the formation of characteristic –C=N bond in **III** and **IV** confirms the imine bond formation. This was further corroborated by the Solid state ^{13}C NMR spectrum for **III** and **IV.** In the case of compound **III**, the HRMS spectrum shows a prominent peak at m/z 599.2690 (calc. 599.2699) which corresponds to $[M+H]^+$ ion peak (Fig. S8, ESI†).

UV-Vis absorption and PL studies of compounds **III** and **IV** are carried out in the DMSO medium. The absorption maximum for compounds **III** and **IV** appeared at 325 nm and 330 nm, respectively, due to the presence of hydroxyl functionalized conjugated TPE moieties (Fig. S9A and Fig. S13A, ESI†). The respective PL spectrum for compounds **III** and **IV** exhibits a maximum at 432 nm and 435 nm when excited at 365 nm (Fig. S9B and Fig. S13B, ESI†).

To get more details about morphology, FE-SEM and TEM images are recorded for compound **IV**. SEM images show the well-organized spherical morphology, with an average particle size of ~100 to 200 nm (Fig. 1F), and the TEM images also suggest the perfect spherical image (Fig. 1H). Furthermore, the DLS study also shows the similar size of the particle for compound **IV** which is observed from FE SEM and TEM analysis (Fig. S11, ESI†). In the case of compound **III,** the FE-SEM image shows aggregate-like structural morphology (Fig. S10, ESI†). The thermal stability of the polymeric compound **IV** was monitored by thermogravimetric (TGA) analysis. TGA data suggest that there is no considerable weight loss up to 350^o C. The sharp weight loss was observed after 400 ^{o}C heating (Fig. S14, ESI†) due to the decomposition of compound **IV**. This ensures the stability of the compound at or below 350^o C. XPS study was conducted to elucidate the chemical composition of the polymeric material. The XPS survey spectrum (Fig. 1B) shows three characteristic peaks: C 1s (284.9 eV), N 1s (399.1 eV), and O 1s (530.21 eV); this confirms the presence of these

elements in **IV**. The deconvoluted C 1s fine spectrum (Fig. 1C) was to reveal three peaks that correspond to sp^2 carbons (C=C, 283.5 eV), mixed carbons (C-C/C=C, 284.40 eV and carbon attached with attached with hydroxyl groups (C=O, 287.35 eV) (Fig. 1C). The N1s spectrum (Fig. 1D) shows two peaks at 398.88, 403.32 eV represent C=N linkages and the protonated amine within the structural backbone. For O 1s the peaks at 532.36 eV appear due to C-OH functionality (Fig. 1E).

Therefore, all the characteristic data and experimental evidence confirm the formation of the new compounds **III** and **IV** respectively.

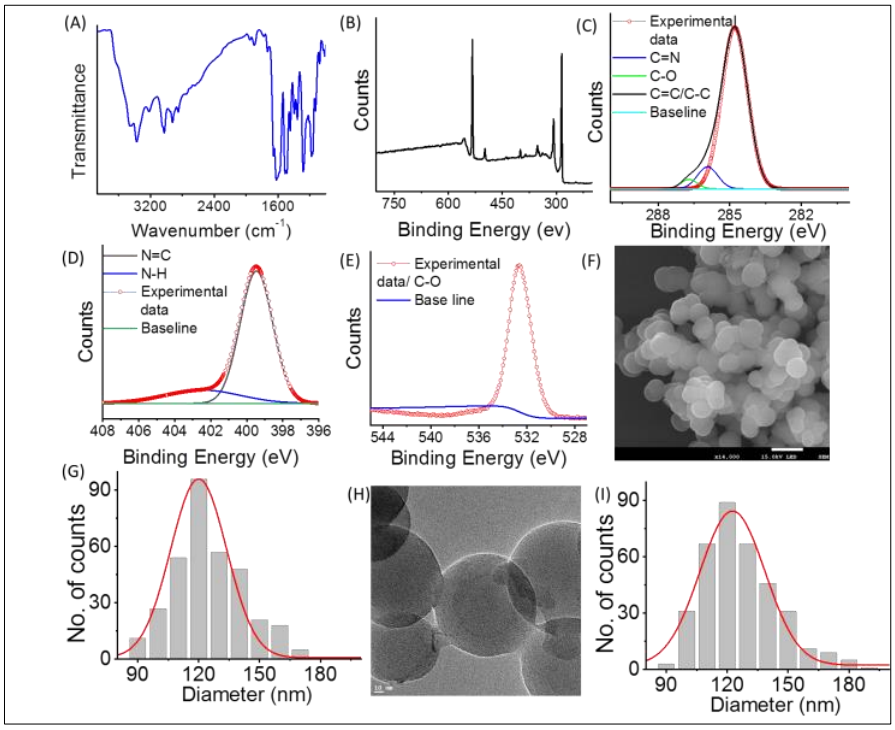

Fig. 1 Characteristic data of compound **IV:** (A) IR-data, (B) XPS analysis of the full spectrum and the high-resolution X-ray photoelectron spectra for (C) C 1s, (D) N 1s, and (E) O 1s. (F) FE-SEM images and their distribution (G), (H) TEM images and their distribution (I).

Chemical sensing studies:

After successful synthesis of receptors **III** and **IV**, we investigated the sensing studies towards TKX 50 as both the compounds share a similar structural core. UV-Vis and PL spectra for compounds **III** and **IV** in the presence of TKX 50 are recorded and compared with those of **III** and **IV** (Fig. S15, and Fig. S16, ESI†) in DMSO. In the case of compound **III**, it has been observed that there is no significant change in absorption spectra in the presence of TKX 50 (Fig. S15A, ESI†). Also, PL studies with compound **III** fail to such enhancement in emission intensity (Fig. S15B, ESI†). The absorption and PL study of **IV** and in the presence of TKX 50 show a substantial change in their characteristic spectrum (Fig. S16, ESI†). Importantly, similar PL with other secondary and nitro explosives (CL-20, HMX, TKX-50, FOX-7, RDX, TNT, TATB, PETN etc.) even in the presence of 100 equivalent as compared to receptor **IV** in DMSO solvent system fail to show any such enhancement in the respective PL spectrum (Fig. 2A). Similarly, to check sensitivity, PL study was performed of **III** towards

other explosives but it is unable to show any selectivity or response (Fig. S17, ESI†). Hence, control compound **III** is not efficient in detecting any explosive by changing its luminescence intensity.

At that moment, we carried out UV-Vis absorption and PL titration experiments of **IV** as host with TKX 50 as a guest. UV-Vis spectra for IV in the presence of increase [TKX-50] (0 to 0.455 μM) show a slight decrease in absorbance in the region 345 to 400 nm and a monotonous increase in the region ~ 320 nm (Fig. 2B). Control study (UV-Vis) with pure TKX-50 in DMSO show that TKX-50 has no detectable absorbance > 300 nm (Fig. S18, ESI†). Thus, this growth in absorbance < 325 nm was not due to the enhanced [TKX-50]. Further, the presence of the isosbestic point at 335 nm suggests the formation of a new adduct that exists in equilibrium with receptor **IV** and TKX-50. As discussed earlier, compound **IV** shows a weak and poorly structured PL spectrum having luminescence maxima at 412 and 431 nm in DMSO following excitation at 365 nm. A titration profile (Fig. 2C) clearly shows that on gradual increase in [TKX-50] (0 to 0.455 μM)) a systematic increase in emission bands at 412 and 435 nms is observed. An Increase in luminescence at 465 nm as a shoulder is also observed. An enhancement of about 18 to 20 times is observed for all three wavelengths, e.g. 412, 435, and 465 nms. Using the intensity data at 435 nm from the titration profile, an association constant for the adduct formation between **IV** and TKX 50 is evaluated using Benesi-Hildebrand (B-H) plot.[10] The evaluated association constant is found to be 2.41x 10^3 M^{-1} (Fig. 2D). TPE is a typical molecular rotor and any restriction in the C-C bond rotation between a $C_{CH=CH}$ and a phenyl ring would be attributed to a luminescence enhancement. This presumably accounts for the luminescence enhancement of **IV** in the presence of TKX-50.

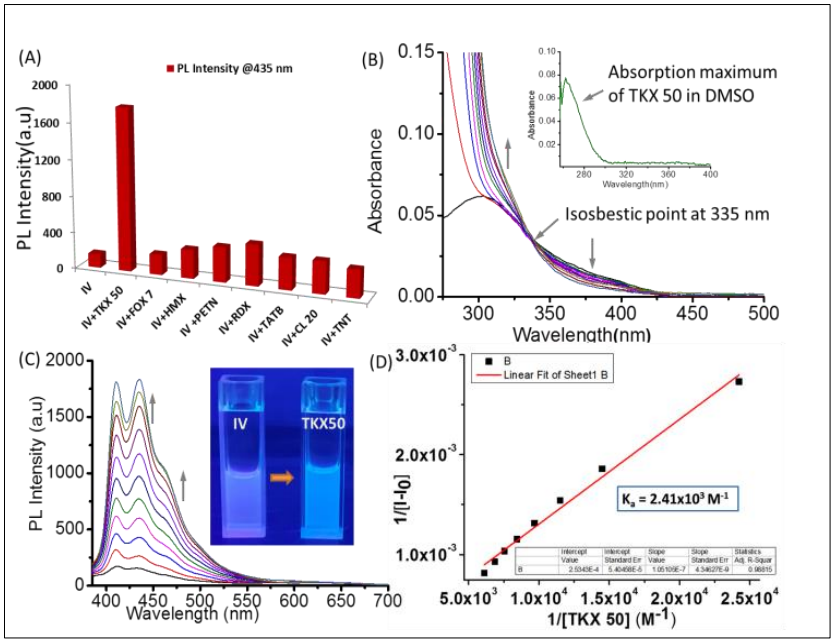

Fig. 2 (A) PL intensity at 435 nm of **IV** (0.5 μM) in presence of various explosive (100 equiv.) in DMSO, excitation at 365 nm, (B) UV-Vis titration spectra **IV** (0.5 μM) with TKX 50 (0.5 mM) (100 equiv.) in DMSO medium, (inset picture: UV-Vis spectrum of TKX 50 in DMSO),

(C)Emission titration spectra of **IV** (0.5 μM) with TKX 50 (0.5 mM) (100 eq) in DMSO medium, excitation at 365 nm, and (D) Benesi-Hildebrand plot for the calculation of association constant from the PL titration experiment.

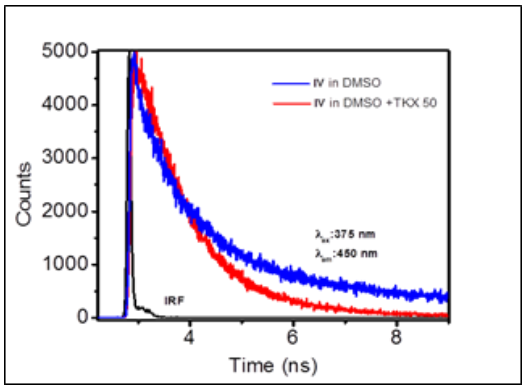

Fig. 3 Pico-second resolved fluorescent transients of the interaction of TKX-50 with Compound **IV** in DMSO solvent.

We have also checked morphological changes due to the interaction between compound **IV** and TKX 50 through the FE-SEM study. It is observed from FE-SEM images that the spherical morphology of compound **IV** converted to aggregate-like morphology due to the interaction between compound **IV** and TKX 50 (Fig. S20, ESI†). Furthermore, TCSPC analysis was performed for **IV** and **IV** with TKX 50 which is shown in Fig. 3 to understand the fluorescence lifetimes.

To investigate the solvent effect on the excited state non-radiative charge transfer (NRCT) process,[11] steady-state absorption and emission spectra of **IV** in various solvents with different polarities were recorded as shown in Figure 5. The absorption of the polymeric compound **IV** exhibits a single absorption band and experiences a slight spectral shift with increasing solvent polarity (Methanol>Acetonitrile>DMSO>Chloroform>Toluene), indicating the occurrence of intramolecular charge transfer (ICT) mechanism. The lower emission intensity of **IV** at different solvents is also indicated in the NRCT process. The fluorescence peak at 435 nm may be attributed to the locally excited (LE) state and the charge transfer state may be connected with inter-system crossing (ISC).[12] In the relatively non-polar solvent (toluene and chloroform) there is little or no interaction between the solvent molecules and the fluorophore **IV**, leaving the fluorophore mostly in the LE state. However, in relatively more polar solvents like acetonitrile and methanol, the fluorophore participates in the excited state charge transfer process with the solvent molecules. Due to the inhibition of the LE state in the relatively polar solvents, the fluorescence intensity of the fluorophore is reduced.

The explanation of the lower fluorescence quantum yield of the fluorophores in the polar solvents is further supported by our picosecond resolved fluorescent transients of the compound **IV** in different solvents at λ_{em} 435 nm with λ_{ex} 375 nm. The fluorescent time profiles were fitted using the multi-exponential decay function following equation 1. The corresponding time constant values are listed in Table 1. As shown in Figure 5C with

increasing polarity of the solution, the average lifetime of the fluorophore decreases consistent with higher NRCT. The shorter time constant (τ_1) in the relatively non-polar solvents (Toluene and chloroform) is associated with a rise component of ~20-30 ns, signifying ultrafast internal conversion to LE state with 435 nm emission. However, in the more polar environment, due to NRCT of the fluorophore, the fluorescence lifetime shows a faster component of ~100 ps consistent with efficient NRCT and a relatively lower possibility of LE state formation. We have shown the mechanistic pathway of NRCT in Fig. 6.

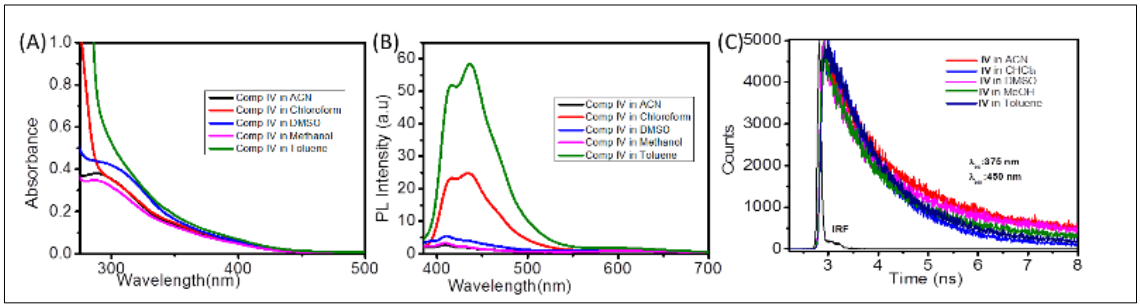

Fig. 5 (A) Absorption spectra of **IV** (2.5 μM) in different solvents, (B) Emission spectra of **IV** (2.5 μM) in different solvents, excited at 365 nm (C) Pico-second resolved fluorescent transients in different solvents, excitation at 375 nm.

Table 1: The corresponding time constant values of comp **IV** in various medium

System	Em (nm)	τ_1 (ps)	τ_2 (ps)	τ_3 (ps)	τ_4 (ps)
IV in MeOH	450		100.2 (28.8%)	888.7 (57.6%)	4400.8 (13.6%)
IV in ACN	450		130.2 (23%)	1019.3 (55.7%)	4858.4 (21.3%)
IV in DMSO	450		140.2 (38.8%)	1038.0 (46.3%)	5748.1 (14.9%)
IV in $CHCl_3$	450	-18.2 (23%)		969.8 (73%)	3427.5 (4%)
IV in Toluene	450	-28.2 (58.7%)		905.4 (35%)	2899.0 (6.3%)
IV with TKX 50	450	-30.8 (16.2%)		885.0 (76.5%)	2234.5 (7.6%)

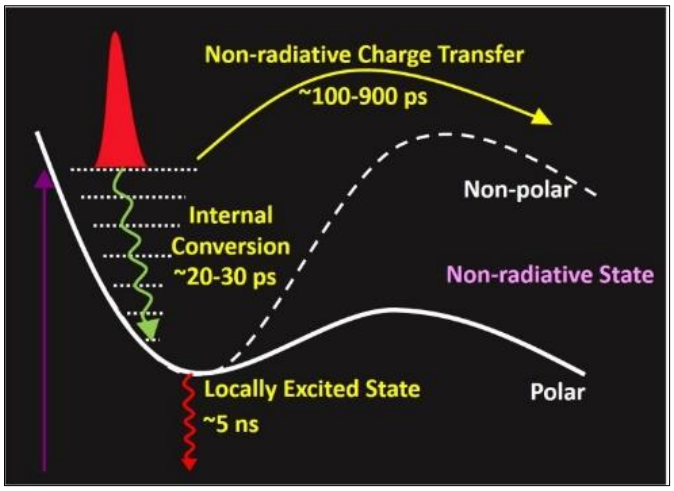

Fig 6. Pictorial representation of the mechanistic pathway for fluorescence response via NRCT process.

Upon interaction of compound **IV** with TKX 50, we have observed that the NRCT processes have significantly been hindered in the excited state revealing excited state relaxation almost similar to the polar solvents (Table 1). It is evident that TKX 50 molecules interrupt the NRCT process and are attributed to the fluorescence 'ON' response. Our conclusion is duly supported by the higher fluorescence yield of the fluorophore and longer relaxation in the pico-second resolved relaxation in the time-resolved emission studies (Fig. 3).

It is worth mentioning that in literature on sensing of explosives is mostly limited to the use of conventional nitroaromatics, which typically have lower LUMO energy levels and allow a luminescence quenching response due to an efficient photoinduced electron transfer process. Such recognition processes are ideally not suited, as these do not allow a favorable signal-to-noise ratio for the lower explosive concentration. Further, such studies rarely involve critical explosives like TKX 50. Hence, sincere efforts have been given to develop a smart hand-held electronic device that would enable us to monitor the presence of TKX 50 through luminescence ON response and by converting such optical responses to a digital output through an electronic device. Importantly, this device can also use an Internet of Things (IoT) enabled for monitoring sample analysis from a remote site. Hence, for instant detection of explosive material like TKX-50, a miniaturized and portable prototype has been designed and constructed based on the developed sensor. The schematic diagram of the prototype is depicted in Figure 7. A cuvette holder of square shape for cuvettes of 10 mm path length has been customized with a light source to excite the sample inside the cuvette and a spectrometer to collect the fluorescence response of the sample upon excitation. As the excitation light source, a UV LED (DC 3 V, 500 mA) of 365 nm wavelength is used in the perpendicular position of the cuvette holder concerning the micro-spectrometer (Hamamatsu C12880MA) detector. The operation of this optical compartment is controlled by an ESP32-based microcontroller unit. The micro-spectrometer and light source are directly connected with defined pins of the micro-controller board ensuring the automatic

data acquisition (DAQ) and visualization of the results. This microcontroller also directs the chronology of switching, illumination time, integration time of the microspectrophotometer, intensity adjustments by automatic Pulse Width Modulation (PWM) of the source, and other features. A 1.14-inch TFT color display at a slanting position in front of the device shows the results. The developed prototype is IoT enabled which pushes data to the cloud using the in-built wi-fi to ensure data transmission from a remote location. The optical spectroscopy-based device is operated using a single push switch button at the top including the data pushing to the cloud. A rechargeable battery source (3000 mAH) has been attached for the supply of power.

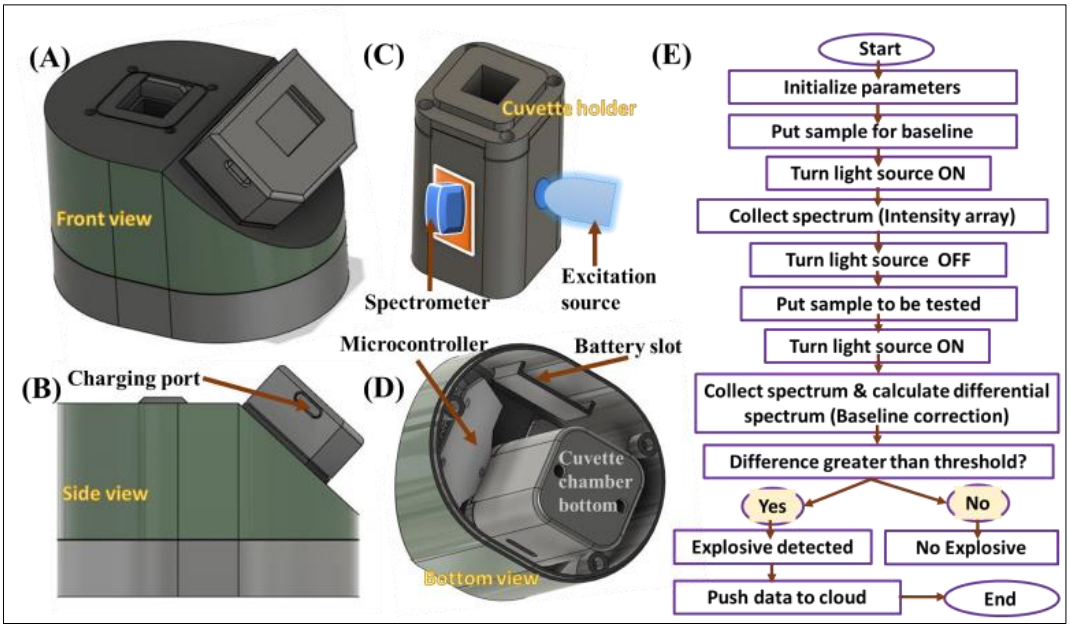

Fig. 7 Schematic diagram of the developed prototype for detection of explosive (A) Front view of the device, (B) side view of the device, (C) the cuvette holder with the excitation light source and micro-spectrometer detector (D) bottom view of the device (E) program flow diagram of the prototype.

Upon powering up, after initialization, the indigenously developed software (in the ARDUINO platform) guides the user to insert a 2 ml sample (**IV** in DMSO) for baseline correction. Then the GUI directs to place the sample to be tested for explosives inside the cuvette holder slot of the device. Next, the device automatically detects the presence of the explosive using the fluorescence response of sample **IV** at the maxima of the emission spectra and predetermined threshold criteria after baseline correction. Finally, by pressing the switch twice, the results can be transmitted to the cloud and stored. The algorithm of the developed device has been illustrated in the flow diagram of Figure 7E. Here, we have attached the practical output of the signal of the prototype in the presence of compound **IV** with TKX 50.

Fig. 8 Working procedure of the developed prototype for detection of TKX 50 *via* visual response.

Conclusions

In summary, we have developed a unique TPE-OH-based polymeric compound that shows a switch ON fluorescence response on binding to TKX 50. Importantly, interference studies show the specificity of this reagent—in terms of fluorescence response—towards TKX 50 over other common, as well as higher explosives. Detailed spectroscopic, analytical, electron microscopic, and light scattering for size distribution are performed to ensure the desired purity and morphology of the polymeric receptor. Steady-state and time-resolved fluorescence studies confirm that binding of TKX 50 effectively interrupts the non-radiative deactivation process that is operational in native TPE-OH-based polymeric receptor **IV** and this is attributed to a fluorescence ON response. Furthermore, a smart IoT-based device has been developed, allowing the integration of optical responses into a digital output. This lightweight portable device enables IoT-based remote detection and is appropriate for surveillance applications.

Experimental section

Materials and method

All commercially available reagents and deuterated solvents were used as received without further purification. Solvents were distilled and dried over molecular sieves. The entire explosives such as CL-20, HMX, TKX-50, FOX-7, RDX, TNT, TATB, and PETN were used for spectroscopic studies and were stored in a vacuum desiccator at low temperatures before use. ^{1}H, ^{13}C NMR spectra were measured on an FT-NMR Bruker/Jeol DPX 400/500 MHz NMR spectrometer. The electronic spray ionization (ESI) mass spectra were recorded on a Xevo G2-XS QTof Mass spectrometer in positive ion mode. FT-IR spectra (4000–400 cm^{-1}) of the compounds were recorded with a PerkinElmer FT-IR spectrometer spectrum Two using the KBr pellet technique. X-ray photoelectron spectra (XPS) were acquired using a Thermo Fischer Scientific ESCALAB XI^{+} instrument equipped with an Al Kα X-ray source ($h\nu$ = 1486.6 eV). The measurements were conducted in a base vacuum operating at 300 W. The analysis of all XPS spectra was performed using Casa XPS software. FE-SEM images were recorded

using a JEOL JSM-7100F instrument operated at 18 kV accelerating voltage. TEM images were also collected on a JEOL JEM-2100 electron microscope operating at 200 kV accelerating voltage.

Steady-state measurements and Time-resolved studies

The steady-state absorption and emission spectra were recorded using a JASCO V-750 spectrophotometer (with a quartz cuvette of path length 1 cm) and a JASCO FP-8200 fluorimeter, respectively. Picosecond resolved fluorescence transients were measured by using time-correlated single-photon counting (TCSPC) setup Edinburgh instrument, U.K. (instrument response function (IRF) of ~80 ps) using a 375 nm excitation laser source. A quartz cuvette of path length 1 cm was used for all the optical measurements. All the time-resolved fluorescence transients were fitted to a function

$$equalX(t) = \int_0^t E(\acute{t})R(t - \acute{t})\, d\acute{t} \quad (1)$$

***Caution*:** Explosive compounds should be used with extreme caution and carefully handled in small quantities only.

Experimental procedures:

Synthesis of **compound I:**

The compound **I** was prepared following McMurry coupling according to the literature procedure with high yield. Characteristic spectra were precisely matched with the literature-reported data.[9]

Synthesis of **compound II:**

Compound **I** (729 mg, 2 mmol) was added to a solution of hexamethylene tetraamine (1.40 g, 10 mmol) in trifluoroacetic acid (TFA) (20 ml) at a stirring condition. The resulting mixture was refluxed for 5 hours. After refluxing, cool to room temperature (RT), and the reaction mixture was quenched with water. It was extracted with $CHCl_3$ and water. The organic phase was washed with saturated sodium carbonate, and brine solution respectively. The organic solvent was dried over sodium sulfate and evaporated to dryness. The resulting compound was purified with silica gel column chromatography using petroleum ether: ethyl acetate as eluent. The product was collected in pure form in 55% yield (462 mg).

HRMS (ESI-MS) for {$C_{28}H_{21}O_4$ = [Comp **II** + H]$^+$} calcd, *m/z* = 421.1440; found, *m/z* =421.1447. ^{1}H NMR (600 MHz, DMSO-d_6): δ (ppm) 6.73 (d, 2H, *J* = 8.4 Hz, Ar-*H*), 6.99-7.01 (m, 4H, - Ar-*H*), 7.05-7.07 (m, 2H, - Ar-*H*), 7.11-7.17 (m, 6H, Ar-*H*), 7.21 (d, 2H, *J* = 2.4 Hz, Ar-*H*), 10.09 (s, 2H, -*CHO),* 10.67 (s, 2H, -*OH)*. ^{13}C NMR (100 MHz, $CDCl_3$): δ (ppm) 117.2, 120.3, 127.4, 128.1, 128.5, 131.3, 131.4, 135.3, 136.4, 139.4, 140.1, 142.8, 160.4, 196.6. IR (KBr) ν= 548, 614, 692, 763, 1147, 1199, 1283, 1472, 1582, 1667, 3390 cm^{-1}.

Synthesis of **compound III:**

Compound **II** (84 mg, 0.2 mmol), 4-Aminotoluene (43 mg, 0.4 mmol), and a catalytic amount (5 wt%) of acetic acid were dissolved in ethanol (20 mL) and stirred at 70-75°C temperature under N_2 atmosphere. After 12 hours of stirring, a yellow color precipitate was separated. The reaction mixture was filtered, washed with methanol, and dried in vacuo. The crude product was purified by soxallation, which produced a solid pale yellow product as compound **III** (80%, 96 mg).

HRMS (ESI-MS) for {$C_{42}H_{35}N_2O_2$ = [Comp **IV** + H]$^+$} calcd, *m/z* = 599.2699; found, *m/z* =599.2690. ^{1}H NMR (400 MHz, DMSO-d_6): δ (ppm) 2.31 (s, 6H, - *CH*$_3$), 6.70 (d, 2H, *J* = 8.8 Hz - *CH*$_2$), 6.96-6.99 (m, 2H, -Ar-*H*), 7.05-7.07 (m, 4H, -Ar-*H*), 7.13-7.19 (m, 6H, -Ar-*H*), 7.21-7.24 (m, 6H, Ar-*H*), 7.25-7.28 (m, 4H, - Ar-*H),* 8.75 (s, 2H, *-OH),* 13.24 (s, 2H, *-NH)*. ^{13}C NMR (100 MHz, DMSO-d_6): δ (ppm) 20.6, 116.2, 118.8, 121.2, 121.3, 126.7, 128.1, 129.9, 129.9, 130.9, 134.2, 134.4, 135.7, 136.6, 139.3, 143.1, 145.1, 159.0, 162.1. IR (KBr) ν= 529, 698, 750, 822, 1133, 1173, 1277, 1354, 1484, 1620 (–C=N), 2908, 3038, 3415 cm^{-1}.

Synthesis of **compound IV:**

Compound **IV** was synthesized following a similar synthetic procedure to compound **III**. 1,3,5-tris(4-aminophenyl)benzene (70 mg, 0.2 mmol), compound **II** (126 mg, 0.3 mmol) and a catalytic amount (5 wt%) of acetic acid were taken in a round bottom flask in 20 ml ethanol. The reaction mixture was stirred at 70-75°C temperature under N_2 for 24 h. A precipitate was observed and separated via filtration. The crude product was washed by methanol, and dried in a vacuum. The crude solid was further purified by soxallation, which produced a solid pale orange product as compound **IV** With a High Yield.

IR (KBr) ν= 542, 626, 698, 756, 822, 1179, 1283, 1354, 1446, 1504, 1617(–C=N), 2928, 3026, 3376 cm^{-1}.

Conflicts of interest

There are no conflicts to declare.

Acknowledgments

A. Das gratefully acknowledges the Defence Research and Development Organisation (DRDO-DMSRDE-TR/0569/CARS), SERB (India) Grants, and JCB/2017/000005 for supporting this research for financial support. S. Bej acknowledges the DRDO for the Research Associate fellowship and IISER Kolkata for the facility of the instrument. S. Dutta acknowledges IISER Kolkata for financial support. S. S. Pasha acknowledges CSIR for financial support.

References

1. (a)J. Zhang, L. A. Mitchell, D. A. Parrish and J. n. M. Shreeve, *J. Am. Chem. Soc.*, 2015, **137**, 10532-10535; (b)N. Fischer, D. Fischer, T. M. Klapoetke, D. G. Piercey and J. Stierstorfer, *J. Mater. Chem.*, 2012, **22**, 20418-20422.

2. (a)T. M. Klapotke, S. Cudzilo, W. A. Trzcinski, J. Paszula, L. Bauer, C. Riedelsheimer and J. T. Lechner, *Propellants, Explos., Pyrotech.*, 2023, **48**, e202300010; (b)Q. An, T. Cheng, W. A. Goddard and S. V. Zybin, *J. Phys. Chem. C*, 2015, **119**, 2196-2207.
3. T. M. Klapotke, S. Cudzilo and W. A. Trzcinski, *Propellants, Explos., Pyrotech.*, 2022, **47**, e202100358.
4. (a)J. Jia, Y. Liu, S. Huang, J. Xu, S. Li, H. Zhang and X. Cao, *RSC Adv.*, 2017, **7**, 49105-49113, (b) N. Fischer, T. M. Klapotke, S. M. Musanic, J. Stierstorfer and M. Suceska, *New Trends Res. Energ. Mater.*, 2013, **16**, 574–585.
5. X. Chen, X. Zhang, H. Wang, L. Zhang and J. Zhu, *Chem. - Eur. J.*, 2023, **29**, e202203605.
6. K. C. To, S. Ben-Jaber and I. P. Parkin, *ACS Nano*, 2020, **14**, 10804-10833.
7. (a)X. Sun, Y. Wang and Y. Lei, *Chem. Soc. Rev.*, 2015, **44**, 8019-8061; (b)S. C. Rickert, S.-X. L. Luo, J. Bahr, J. Kohn, M. Xue, A. Hansen, S. Grimme, S.-S. Jester, T. M. Swager and S. Hoeger, *J. Am. Chem. Soc.*, 2024, **146**, 2986-2996; (c)J. Gao, X. Chen, S. Chen, H. Meng, Y. Wang, C. Li and L. Feng, *Anal. Chem.*, 2019, **91**, 13675-13680; (d)W. Wu, N. Shi, J. Zhang, X. Wu, T. Wang, L. Yang, R. Yang, C. Ou, W. Xue, X. Feng, L. Xie and W. Huang, *J. Mater. Chem. A*, 2018, **6**, 18543-18550; (e)L. Mosca, S. Karimi Behzad and P. Anzenbacher, *J. Am. Chem. Soc.*, 2015, **137**, 7967-7969; (f)C. Wang, J. Shang, Y. Lan, T. Tian, H. Wang, X. Chen, J.-Y. Gu, J. Z. Liu, L.-J. Wan, W. Zhu and G. Li, *Adv. Funct. Mater.*, 2015, **25**, 6009-6017; (g)T. L. Andrew and T. M. Swager, *J. Am. Chem. Soc.*, 2007, **129**, 7254-7255; (h)A. Yildirim, H. Acar, T. S. Erkal, M. Bayindir and M. O. Guler, *ACS Appl. Mater. Interfaces*, 2011, **3**, 4159-4164; (i)D. Li, J. Liu, R. T. K. Kwok, Z. Liang, B. Z. Tang and J. Yu, *Chem. Commun.*, 2012, **48**, 7167-7169; (j)M. Faheem, S. Aziz, X. Jing, T. Ma, J. Du, F. Sun, Y. Tian and G. Zhu, *J. Mater. Chem. A*, 2019, **7**, 27148-27155; (k)A. Raeupke, A. Palma-Cando, E. Shkura, P. Teckhausen, A. Polywka, P. Goerrn, U. Scherf and T. Riedl, *Sci. Rep.*, 2016, **6**, 29118.
8. T. Singha Mahapatra, A. Dey, H. Singh, S. S. Hossain, A. K. Mandal and A. Das, *Chem. Sci.*, 2020, **11**, 1032-1042.
9. (a)K. Li, G. Jiang, F. Zhou, L. Li, Z. Zhang, Z. Hu, N. Zhou and X. Zhu, *Polym. Chem.*, 2017, **8**, 2686-2692; (b)W. Z. Yuan, Z.-Q. Yu, Y. Tang, J. W. Y. Lam, N. Xie, P. Lu, E.-Q. Chen and B. Z. Tang, *Macromolecules*, 2011, **44**, 9618-9628.
10. M. S. Thippeswamy, L. Naik, C. V. Maridevarmath, H. M. Savanur and G. H. Malimath, *J. Mol. Struct.*, 2022, **1264**, 133274.
11. H. Qu, X. Tang, X. Wang, Z. Li, Z. Huang, H. Zhang, Z. Tian and X. Cao, *Chem. Sci.*, 2018, **9**, 8814-8818.
12. D. Zhong, S. K. Pal and A. H. Zewail, *ChemPhysChem*, 2001, **2**, 219-227.